

Geometrical information in soft-x-ray appearance potential spectroscopy and Auger-electron appearance potential spectroscopy

G. E. Laramore

Division of Radiation Oncology, University of Washington Hospital, Seattle, Washington 98105

(Received 19 December 1977; revised manuscript received 27 July 1978)

A general formalism is presented for the calculation of geometrically induced structure in soft-x-ray appearance potential spectroscopy and Auger-electron appearance potential spectroscopy spectra. Electronic wave functions similar to those used in low-energy-electron diffraction theory are used to describe the incident electron and the excited-final-state electrons. The problem of calculating the excitation matrix element is discussed, and its relevant symmetry properties displayed. Model calculations assuming a constant "bare" excitation matrix element, a spherically symmetric electronic density of states, and *S*-wave scattering from the ion cores are performed for a cluster of nickel atoms and for a cluster that models oxygen on a Ni(001) surface. These calculations exhibit the general features predicted by the formalism. In the context of this study, it appears that multiple-scattering effects will be important in any analysis of experimental data that requires a direct comparison with theoretical calculations.

I. INTRODUCTION

In recent years there has been considerable interest in using atomic core-level excitation techniques to obtain information about the local geometrical structure in the neighborhood of given atoms. Two such techniques are energy- and angle-resolved photoemission from localized electronic states¹⁻⁴ and extended x-ray absorption fine structure (EXAFS) measurements.⁵⁻¹⁰ In these two techniques high-energy photons are used to excite electrons from localized atomiclike levels and the scattering of the final-state electrons from neighboring atoms produces interference phenomena in the measured spectra from which information about the local atomic geometry can be obtained. Theoretical calculations of these effects use the electronic wave functions developed from low-energy-electron diffraction (LEED) work^{11,12} to describe the final-state electrons. In the photoemission work the excited atom acts like a localized source of electrons which are then directly observed after scattering from the neighboring atoms. In EXAFS one does not observe the excited electrons directly but rather observes oscillations in the x-ray absorption coefficient. Hence, in effect one sees an angular average over the allowed final-state wave functions. These techniques are not restricted to ordered structures but can be used to probe the local atomic geometries in disordered solids and in complex biological proteins. One picks the site of interest by the particular core level that is excited. These probes thus complement LEED and x-ray scattering which require ordered systems. The main disadvantage of these probes is that they require use of a synchrotron storage ring in order

to obtain a sufficiently high intensity continuum photon source to make the experimental measurements feasible.

Soft-x-ray appearance potential spectroscopy (SXAPS)¹³⁻¹⁶ and Auger-electron appearance potential spectroscopy (AEAPS),^{16,17} on the other hand, require only relatively simple and inexpensive equipment for their undertaking and have the potential for yielding the same sort of geometrical information as obtained from EXAFS. In SXAPS one monitors the *total* x-ray emission from an electron-bombarded sample as a function of the incident-beam energy. One finds distinct structure corresponding to core-level excitations superimposed upon a bremsstrahlung background. This structure can be enhanced by potential-modulation techniques, i.e., by differentiating with respect to the incident-beam energy. In AEAPS one monitors the *total* electron current to the sample as a function of the incident-beam energy. Structure corresponding to Auger processes as the core level deexcites is superimposed upon a background current and, as in the case of SXAPS, this structure can be enhanced by potential-modulation techniques. Since the x rays or the emitted electrons are *not* energy resolved, one essentially measures the probability of exciting the core-level state. In the past these techniques have been used primarily to obtain information about surface chemical composition and about the unoccupied electronic states near the Fermi level. However, away from threshold there should be structure which is determined primarily by the atomic geometry in the neighborhood of the excited atom.¹⁸ Although the experimental techniques are fairly straightforward and do not require sophisticated equipment, their theoretical interpretation

is in at least three respects more complicated than in the case of photoemission or EXAFS: (i) A high-energy electron rather than a photon is used to excite the core level and so one must include scattering processes in the initial as well as the final state. (ii) There are two final-state electrons and so calculation of the core-level excitation probability involves a sum over final-state energies rather than the electron final-state energy being determined simply by energy conservation. (iii) There is no definite selection rule which relates the angular-momentum quantum numbers of the final-state electrons to those of the initial core state. This paper represents a first step in addressing these problems.

In Sec. II, I describe the formalism used to address the problem and present a general expression for the transition rate in terms of the scattering phase shifts of the individual atoms. In Sec. III, I specialize to the case of *S*-wave scatterers and present the results of model calculations for systems having other parameters appropriate to bulk nickel and to the O-Ni(001) system. In the context of these model calculations, it appears that multiple-scattering effects make significant changes in the calculated spectra. Finally, I summarize my results in Sec. IV.

II. FORMALISM

The Hamiltonian describing the system can be written as

$$H = H_0^e + H_0^i + H_1, \quad (2.1)$$

where H_0^e is the Hamiltonian describing the interaction of the initial- and final-state electrons with the background conduction electrons and the other elementary excitations of the solid;

$$H_0^i = \sum_n V_n(\vec{r} - \vec{R}_n) \quad (2.2)$$

describes the interaction between the incident electron and the unexcited system;

$$H_0^f = \sum_n \bar{V}_n(\vec{r} - \vec{R}_n) \quad (2.3)$$

describes the interaction between the final-state electrons and the system containing the core hole; and

$$H_1 = e^2 / |\vec{r} - \vec{r}'| \quad (2.4)$$

is the electron-electron interaction term which describes the excitation of the core electron. Following previous LEED work^{11,12,19,20} I will describe H_0^e phenomenologically in terms of the one-electron Green's function which describes the propagation of the electron between successive collisions with the ion cores, i.e.,

$$G(\vec{k}, E) = \langle \vec{k}' | E - H_0^e + i\eta | \vec{k} \rangle \delta_{\vec{k}\vec{k}'}, \\ = \left(E - \frac{\hbar^2 k^2}{2m} - \Sigma(E) \right)^{-1}. \quad (2.5)$$

In Eq. (2.5), η is a positive infinitesimal and $\Sigma(E)$ is a complex proper self-energy,

$$\Sigma(E) = -V_0 - i\Gamma(E). \quad (2.6)$$

In Eq. (2.6)

$$\Gamma(E) = \left(\frac{\hbar}{m\lambda_{ee}} \right) \left(\frac{2mE}{\hbar^2} + \frac{2mV_0}{\hbar^2} \right)^{1/2} \quad (2.7)$$

describes the damping of the electronic wave function as it propagates in terms of the mean-free-path parameter λ_{ee} . In Eqs. (2.2) and (2.3) $V_n(\vec{r} - \vec{R}_n)$ and $\bar{V}_n(\vec{r} - \vec{R}_n)$ describe the interaction between the propagating electron and the n th ion core, respectively, for the unexcited and the excited system. For simplicity, I will not consider explicitly the effects of the lattice vibrations. To lowest order these will simply renormalize the individual electron-atom scattering amplitudes that enter the LEED wave functions used to describe the initial and final electronic states.^{20,21} In addition, there are many-body effects related to the sudden excitation of the core electron²²⁻²⁴ but these should not be important far from threshold where the geometrical effects appear. Here I will follow the approach used in photoemission⁴ and EXAFS⁹ and consider the potential of the excited atom to be specified by removing one electron from the core level in question and distributing it over the muffin-tin sphere to simulate the effects of screening. Thus, the potentials V and \bar{V} are specifiable in terms of atomic charge densities obtained from calculations utilizing a statistical exchange approximation^{25,26} which are overlapped to form muffin-tin potentials. From these effective one-electron potentials, scattering phase shifts specifying the electron-ion-core scattering amplitudes can be determined as in the LEED problem. However, these phase shifts can be different in the initial and final states as, in principle, can be the parameters that enter the definition of $\Sigma(E)$.

My starting point is the following expression for the spin-averaged transition rate for exciting a core electron from a closed atomic shell^{27,28}:

$$\langle \dot{\Phi}_I \rangle_s = \frac{2\pi}{\hbar} N_c \sum_{\vec{k}_f, \vec{k}_f' > P_F} \delta(E_i - E_f - E_{f'} - \Delta) \\ \times \left[\frac{3}{4} |M_{\uparrow\uparrow}^c(\vec{k}_i; \vec{k}_f, \vec{k}_{f'})|^2 + \frac{1}{4} |M_{\uparrow\downarrow}^c(\vec{k}_i; \vec{k}_f, \vec{k}_{f'})|^2 \right], \quad (2.8)$$

where $\langle \rangle_s$ indicates an average over the spin of

the incident electron, N_c is the number of electrons in the atomic shell under consideration, $E_i(\vec{k}_i)$ is the energy (momentum) of the incident electron, $E_f(\vec{k}_f)$ and $E_{f'}(\vec{k}_{f'})$ are the energy (momenta) of the two excited-final-state electrons, Δ is the binding energy of the core electron, and $M_{\uparrow\uparrow}^c$ and $M_{\uparrow\downarrow}^c$ are the respective matrix elements for the two final-state electrons emerging in a parallel or antiparallel spin state. The summation is over all final states with momenta greater than the Fermi momentum P_F . This is a simple generalization of the usual atomic physics expression^{27,28} for electron ionization of helium for the case where the term describing the capture of the incident electron by the atom is neglected. However, instead of using either plane waves or Coulomb wave functions I use LEED-like wave functions to describe both the incident electron and the excited-final-state electrons. The matrix elements $M_{\uparrow\uparrow}^c$ and $M_{\uparrow\downarrow}^c$ are thus related to the "bare" excitation matrix elements of atomic physics $W_{\uparrow\uparrow}^c$ through

$$M_{\uparrow\uparrow}^c(\vec{k}; \vec{k}_1, \vec{k}_2) = \langle \psi_{f'f'} | \vec{k}_1, \vec{k}_2 \rangle_{(\mp)} W_{\uparrow\uparrow}^c(\vec{k}; \vec{k}_1, \vec{k}_2) \langle \vec{k} | \psi_i \rangle. \quad (2.9)$$

In Eq. (2.9) $\langle \vec{k} | \psi_i \rangle$ is the momentum-space representation of the one-electron LEED wave function²⁹

$$\begin{aligned} \langle \vec{k} | \psi_i \rangle &= \delta_{\vec{k}, \vec{k}_i} + G(\vec{k}, E_i) \sum_{n' (n' \neq 0)} \exp(-i\vec{k} \cdot \vec{R}_{n'}) \left(\exp(i\vec{k}_i \cdot \vec{R}_n) t_n(\vec{k}, \vec{k}_i) \right. \\ &\quad + \sum_{\vec{k}_1} \sum_{n' (n' \neq n)} t_n(\vec{k}, \vec{k}_1) \exp[i\vec{k}_1 \cdot (\vec{R}_n - \vec{R}_{n'})] G(\vec{k}_1, E_i) \exp(i\vec{k}_i \cdot \vec{R}_{n'}) t_{n'}(\vec{k}_1, \vec{k}_i) \\ &\quad + \sum_{\substack{n'' (n'' \neq n) \\ n' (n' \neq n')}} \sum_{\vec{k}_1, \vec{k}_2} t_n(\vec{k}, \vec{k}_1) \exp[i\vec{k}_1 \cdot (\vec{R}_n - \vec{R}_{n''})] \\ &\quad \times G(\vec{k}_1, E_i) t_{n''}(\vec{k}_1, \vec{k}_2) \exp[i\vec{k}_2 \cdot (\vec{R}_{n''} - \vec{R}_{n'})] \\ &\quad \left. \times G(\vec{k}_2, E_i) \exp(i\vec{k}_i \cdot \vec{R}_{n'}) t_{n'}(\vec{k}_2, \vec{k}_i) + \dots \right) \\ &\equiv \delta_{\vec{k}, \vec{k}_i} + G(\vec{k}, E_i) \sum_{n, n' (n \neq 0)} \exp(-i\vec{k} \cdot \vec{R}_n) \mathcal{O}_{nn'}(\vec{k}, \vec{k}_i), \end{aligned} \quad (2.12)$$

where $\mathcal{O}_{nn'}(\vec{k}, \vec{k}_i)$ satisfies the integral equation

$$\begin{aligned} \mathcal{O}_{nn'}(\vec{k}, \vec{k}_i) &= \exp(i\vec{k}_i \cdot \vec{R}_n) t_n(\vec{k}, \vec{k}_i) \delta_{nn'} \\ &\quad + \sum_{n'' (n'' \neq n)} \sum_{\vec{k}_1} t_n(\vec{k}, \vec{k}_1) \exp[i\vec{k}_1 \cdot (\vec{R}_n - \vec{R}_{n''})] \\ &\quad \times G(\vec{k}_1, E_i) \mathcal{O}_{n''n'}(\vec{k}_1, \vec{k}_i). \end{aligned} \quad (2.13)$$

In Eq. (2.12), I have taken the excited atom to lie at the origin of my coordinate system and have labeled it by the index $n=0$. The restriction on

$$\begin{aligned} \psi_i(\vec{r}) &= \frac{e^{i\vec{k}_i \cdot \vec{r}}}{(2\pi)^{3/2}} + \int d^3r_1 d^3r_2 G(\vec{r} - \vec{r}_1) \\ &\quad \times T(\vec{r}_1, \vec{r}_2) \frac{e^{i\vec{k}_i \cdot \vec{r}_2}}{(2\pi)^{3/2}}, \end{aligned} \quad (2.10)$$

where $T(\vec{r}_1, \vec{r}_2)$ is the T matrix that describes all possible multiple-scattering paths that begin at point \vec{r}_2 and end at point \vec{r}_1 . The evaluation of the momentum transform of $T(\vec{r}_1, \vec{r}_2)$ is the object of LEED theory and it is not my intention to repeat here the substantial body of work that has gone into this. However, some modifications of the formalism are advantageous in performing the sum over final states and these will be briefly described.

$$\begin{aligned} \langle \vec{k}_2, \vec{k}_1 | \psi_{f'f'} \rangle_{(\mp)} &= \frac{1}{\sqrt{2}} (\langle \vec{k}_2 | \psi_{f'} \rangle \langle \vec{k}_1 | \psi_{f'} \rangle \\ &\quad \mp \langle \vec{k}_1 | \psi_{f'} \rangle \langle \vec{k}_2 | \psi_{f'} \rangle) \end{aligned} \quad (2.11)$$

is an antisymmetric (symmetric) combination of one-electron LEED wave functions and the "bare" excitation matrix elements are simple generalizations of those describing the electron-impact ionization of hydrogen using a plane-wave basis. The form of these bare matrix elements and their relevant symmetry properties will be displayed in the appendix.

In terms of the single-atom elastic-scattering amplitudes, $t_n(\vec{k}_2, \vec{k}_1)$, the momentum transform of Eq. (2.10) can be written as

the sum over n comes about because the LEED wave function for the incident electron includes all multiple-scattering processes *prior* to the excitation of the core-level electron. The Green's function $G(\vec{k}, E_i)$ describes the propagation of the incident electron between its final elastic scattering event at the n th atom and the origin where it excites the given core level. $\mathcal{O}_{nn'}(\vec{k}, \vec{k}_i)$ then represents the sum of all elastic multiple-scattering processes for which the initial event is an electron of momentum \vec{k}_1 scattering from the n' th atom and the final scattering event occurs at the n th atom

with the final momentum being \vec{k} . In Eq. (2.12), the momentum δ function accounts for the process where the incoming electron excites the core electron without any preceding elastic scattering event. The notation of Eqs. (2.10) and (2.12) is that of Duke and Laramore^{20,21,29} and the reader is referred there for a more detailed explanation. The advantage of using the $\phi_{mm'}(\vec{k}, \vec{k}_i)$ matrix as defined by Eq. (2.13) is that the structural Green's functions which enter the calculation of its partial-wave expansion do not explicitly contain the momentum \vec{k}_i . The importance of this will become clearer later on in the calculation. I will

consider first the matrix element for the case where the final-state electrons emerge in a triplet state. As a notational convenience, I will rewrite Eq. (2.12) as

$$\langle \vec{k} | \psi_i \rangle = \delta_{\vec{k}, \vec{k}_i} + G(\vec{k}, E_i) \sum_{n(n \neq 0)} S_n(\vec{k}, \vec{k}_i), \quad (2.14)$$

where

$$S_n(\vec{k}, \vec{k}_i) \equiv \sum_{n'} \exp(-i\vec{k} \cdot \vec{R}_n) \phi_{nn'}(\vec{k}, \vec{k}_i). \quad (2.15)$$

Substituting Eqs. (2.11) and (2.14) into Eq. (2.9) the excitation matrix element becomes

$$\begin{aligned} M_{\uparrow\uparrow}^c(\vec{k}_i; \vec{k}_f, \vec{k}_{f'}) &= \sqrt{2} \left(W_{\uparrow\uparrow}^c(\vec{k}_i; \vec{k}_f, \vec{k}_{f'}) + \sum_{\vec{k}} \sum_n' W_{\uparrow\uparrow}^c(\vec{k}; \vec{k}_f, \vec{k}_{f'}) G(\vec{k}, E_i) S_n(\vec{k}, \vec{k}_i) + \dots \right. \\ &+ \sum_{\vec{k}_1, \vec{k}_2} \sum_{nm_1} \bar{S}_{n_1}^*(\vec{k}_1, \vec{k}_f) G^*(\vec{k}_1, E_f) W_{\uparrow\uparrow}^c(\vec{k}; \vec{k}_1, \vec{k}_{f'}) G(\vec{k}, E_i) S_n(\vec{k}, \vec{k}_i) + \dots \\ &\left. + \sum_{\vec{k}_1, \vec{k}_2} \sum_{nm_1 n_2} \bar{S}_{n_1}^*(\vec{k}_1, \vec{k}_f) G(\vec{k}_1, E_f) \bar{S}_{n_2}^*(\vec{k}_2, \vec{k}_f) G^*(\vec{k}_2, E_{f'}) W_{\uparrow\uparrow}^c(\vec{k}; \vec{k}_1, \vec{k}_2) G(\vec{k}, E_i) S_n(\vec{k}, \vec{k}_i) \right). \quad (2.16) \end{aligned}$$

In Eq. (2.16), \bar{S}_{n_1} indicates that the atomic potentials of the excited final state are to be used in evaluating the final-state wave functions and \sum_n' means that the sum is restricted to $n \neq 0$. The symmetry property [see Eq. (A1) in the Appendix]

$$W_{\uparrow\uparrow}^c(\vec{k}; \vec{k}_1, \vec{k}_2) = -W_{\uparrow\uparrow}^c(\vec{k}; \vec{k}_2, \vec{k}_1) \quad (2.17)$$

has been utilized in obtaining Eq. (2.16). The

next step is to pass to the continuum representation

$$\sum_{\vec{k}} \rightarrow \int \frac{d^3\kappa}{(2\pi)^3} \quad (2.18)$$

and to perform the momentum integrals via a partial-wave expansion. To illustrate this, consider the second term in Eq. (2.16)

$$\begin{aligned} \sum_{\vec{k}} \sum_n' W_{\uparrow\uparrow}^c(\vec{k}; \vec{k}_f, \vec{k}_{f'}) G(\vec{k}, E_i) S_n(\vec{k}, \vec{k}_i) &= \sum_{nn'(n \neq 0)} \int \frac{d^3\kappa}{(2\pi)^3} \sum_L W_{\uparrow\uparrow}^{cL}(\kappa; \vec{k}_f, \vec{k}_{f'}) Y_L(\Omega_\kappa) G(\vec{k}, E_i) \\ &\times \sum_{L_1} 4\pi(i)^{-1} j_{L_1}(\kappa R_n) Y_{L_1}(\Omega_{R_n}) Y_{L_1}^*(\Omega_\kappa) \\ &\times \sum_{L_2 L_3} \phi_{nm}^{L_2 L_3}(\kappa, \kappa_i) Y_{L_2}^*(\Omega_\kappa) Y_{L_3}(\Omega_{\kappa_i}) \\ &= \sum_{mm'(n \neq 0)} \sum_{LL_1 L_2 L_3} I(L; L_1, L_2)(i)^{-1} Y_L(\Omega_{R_n}) \\ &\times \int_0^\infty \frac{d\kappa \kappa^2}{2\pi^2} W_{\uparrow\uparrow}^{cL}(\kappa; \vec{k}_f, \vec{k}_{f'}) G(\vec{k}, E) j_{L_1}(\kappa R_n) \phi_{nm}^{L_2 L_3}(\kappa, \kappa_i) Y_{L_3}(\Omega_{\kappa_i}). \quad (2.19) \end{aligned}$$

In Eq. (2.19)

$$I(L; L_1, L_2) = \int d\Omega Y_L(\Omega) Y_{L_1}^*(\Omega) Y_{L_2}^*(\Omega), \quad (2.20)$$

where L is a shorthand notation for the angular-momentum variables (l, m), $Y_L(\Omega)$ is the spherical-

harmonic function, $j_l(\kappa r)$ is the spherical Bessel function of order l , and

$$\sum_L \equiv \sum_{l=0}^\infty \sum_{m=-l}^l. \quad (2.21)$$

$I(L; L_1, L_2)$ is expressible in terms of the Clebsch-

Gordan coefficients³⁰ and if real analogs of the spherical harmonics are used³¹ then the $I(L; L_1, L_2)$ become the usual Gaunt coefficients. In going to the second term on the right-hand side of Eq. (2.19), the following expansion formulas were used³²

$$\exp(i\vec{k} \cdot \vec{R}_n) = \sum_L 4\pi(i)^L j_L(\kappa R_n) Y_L^*(\Omega_{R_n}) Y_L(\Omega_\kappa); \quad (2.22)$$

$$W_{\uparrow\uparrow}^c(\vec{k}, \vec{k}_f, \vec{k}_{f'}) = \sum_L W_{\uparrow\uparrow}^{cL}(\kappa; \vec{k}_f, \vec{k}_{f'}) Y_L(\Omega_\kappa); \quad (2.23)$$

$$\phi_{mn}^c(\vec{k}, \vec{k}_1) = \sum_{L_2 L_3} \phi_{mn}^{cL}(\kappa, \kappa_1) Y_{L_2}^*(\Omega_\kappa) Y_{L_3}(\Omega_{\kappa_1}). \quad (2.24)$$

The important thing to note about Eq. (2.19) is that for $I(L; L_1, L_2) \neq 0$, the integrand is an even function³³ of κ . Hence, the integral can be extended to $-\infty$ and performed using contour techniques. As in the LEED work,^{20,21} I will include only the contributions from the poles of $G(\vec{k}, E)$ which yields

$$\begin{aligned} & \sum_{\vec{k}} \sum_n' W_{\uparrow\uparrow}^c(\vec{k}; \vec{k}_f, \vec{k}_{f'}) G(\vec{k}, E) S_n(\vec{k}, \vec{k}_i) \\ &= \sum_{mn' (n \neq 0)} \sum_{LL_2 L_3} W_{\uparrow\uparrow}^{cL}(K(E_i); \kappa_f, \kappa_{f'}) G_{on}^{LL} \mathcal{A}(K(E_i)) \\ & \quad \times \phi_{mn'}^{L_2 L_3} \mathcal{A}(K(E_i); \kappa_i) Y_{L_3}(\Omega_{\kappa_i}), \end{aligned} \quad (2.25)$$

where

$$\begin{aligned} M_{\uparrow\uparrow}^c(\vec{k}_i; \vec{k}_f, \vec{k}_{f'}) &= \sqrt{2} \left(W_{\uparrow\uparrow}^c(\vec{k}_i; \vec{k}_f, \vec{k}_{f'}) + \sum_{L_1 n_1}' W_{\uparrow\uparrow}^{cL_1}(K(E_i); \vec{k}_f, \vec{k}_{f'}) \psi_{n_1}^L(K(E_i)) + \dots \right. \\ & \quad + \sum_{L_1 L_2 n_1 n_2}' W_{\uparrow\uparrow}^{cL_1 L_2}(K(E_i); K^*(E_f), \vec{k}_{f'}) \psi_{n_2}^{*L_2}(K(E_f)) \psi_{n_1}^L(K(E_i)) + \dots \\ & \quad \left. + \sum_{L_1 L_2 L_3 n_1 n_2 n_3}' W_{\uparrow\uparrow}^{cL_1 L_2 L_3}(K(E_i); K^*(E_f), K^*(E_{f'})) \psi_{n_2}^{*L_2}(K(E_f)) \psi_{n_3}^{*L_3}(K(E_{f'})) \psi_{n_1}^L(K(E_i)) \right), \end{aligned} \quad (2.29)$$

where the \sum' indicates that the sums over atomic sites are for $n_1, n_2, n_3 \neq 0$.

For the case of antiparallel electron spins the calculation goes through in an analogous manner. This time the final-state wave function in the momentum representation is

$$\begin{aligned} \langle \vec{k}_2 \kappa_1 | \psi_{f, f'} \rangle_{(+)} &= \frac{1}{\sqrt{2}} (\langle \vec{k}_2 | \psi_{f'} \rangle \langle \vec{k}_1 | \psi_f \rangle \\ & \quad + \langle \vec{k}_2 | \psi_f \rangle \langle \vec{k}_1 | \psi_{f'} \rangle). \end{aligned} \quad (2.30)$$

The symmetry property [see Eq. (A9) in the Appendix]

$$W_{\uparrow\uparrow}^c(\vec{k}; \vec{k}_1, \vec{k}_2) = W_{\uparrow\uparrow}^c(\vec{k}; \vec{k}_2, \vec{k}_1) \quad (2.31)$$

compensates for the sign change in the final-state wave function and one obtains

$$(\hbar^2/2m)K^2(E_i) \equiv E_i - \Sigma(E_i) \quad (2.26)$$

and

$$\begin{aligned} G_{n_1 n_2}^{LL} \mathcal{A}(K(E_i)) &\equiv \sum_{L_1} \frac{(-i)^{L_1+1}}{2\pi} \frac{mK(E_i)}{\hbar^2} I(L; L_1, L_2) \\ & \quad \times h_{L_1}^{(1)}(K(E_i) | \vec{R}_{n_2} - \vec{R}_{n_1} |) \\ & \quad \times Y_{L_1}(\Omega_{\vec{R}_{n_2} - \vec{R}_{n_1}}) \end{aligned} \quad (2.27)$$

is the structural propagator which describes the coupling of the L_2 partial-wave component centered at site n_2 to the L partial-wave component centered at site n_1 . In Eq. (2.27) $h_{L_1}^{(1)}$ is the L_1 th spherical Hankel function of the first kind. Note that unlike the structural propagators used in previous LEED work, there is no explicit dependence on \vec{k}_i in Eq. (2.27). The angular dependence of \vec{k}_i enters only through $Y_{L_3}(\Omega_{\kappa_i})$ in Eq. (2.25). The evaluation of the other terms in Eq. (2.16) follow in an analogous fashion. Defining ($n_1 \neq 0$)

$$\begin{aligned} \psi_{n_1}^L(K(E_i)) &\equiv \sum_{L_2 L_3} \sum_{n'} G_{on_1}^{L_2 L_3} \mathcal{A}(K(E_i)) \\ & \quad \times \phi_{n_1 n'}^{L_2 L_3} \mathcal{A}(K(E_i), \kappa_i) Y_{L_3}(\Omega_{\kappa_i}) \end{aligned} \quad (2.28)$$

the excitation matrix element can be written as

$M_{\uparrow\uparrow}^c(\vec{k}_i; \vec{k}_f, \vec{k}_{f'})$ equal to the right-hand side of Eq. (2.29) with

$$W_{\uparrow\uparrow}^c \rightarrow W_{\uparrow\downarrow}^c. \quad (2.32)$$

The Coulomb interaction is spin independent and so for a spin-polarized beam of incident electrons it should be possible in principle (if not in practice) to separately measure the singlet and triplet component of the final-state electrons. However, in the APS measurements, one measures the quality given in Eqs. (2.8).

To proceed further I pass to the continuum limit on the momentum sums and assume a given model for the electronic density of states above the Fermi level. Since the angular dependence of the initial- and final-state wave vectors enters only

via spherical harmonic functions, the angular integrations $d\Omega_f$ and $d\Omega_{f'}$ can be easily carried out on a term by term basis and then the integration over $d\kappa_{f'}$ $\kappa_{f'}^2$ carried out with the aid of the energy δ function. In the case of a disordered solid, one essentially sees an average over the angular components of the incident wave vector and this also is easily performed. The resulting equation contains a large number of terms and is tedious to write down. Since it is model dependent, I will not display it explicitly here but will illustrate it in Sec. III for the special case of S-wave scattering and a spherically symmetric density of states.

It only remains to describe the evaluation of $\mathcal{O}_{nn'}^{L'L'}(K(E_i), \kappa_i)$ and hence $\psi_{n_1}^{L'}(K(E_i))$. Defining

$$p_n(\vec{\kappa}, \vec{\kappa}_i) = \exp(i\vec{\kappa}_i \cdot \vec{R}_n) t_n(\vec{\kappa}, \vec{\kappa}_i) \quad (2.33)$$

$$= \sum_{L'L'} p_n^{L'L'}(\kappa, \kappa_i) Y_{L'}^*(\Omega_{\kappa}) Y_{L'}(\Omega_{\kappa_i}),$$

where

$$p_n^{L'L'}(\kappa, \kappa_i) = \sum_{L_1 L_2} 4\pi(i)^{L_1} I(L'; L_1, L_2) Y_{L_1}^*(\Omega_{R_n}) \times j_{L_2}(\kappa_i R_n) t_n^{L'L_2}(\kappa, \kappa_i). \quad (2.34)$$

The partial-wave components of Eq. (2.24) satisfy the following matrix equation

$$\mathcal{O}_{nn'}^{L'L'}(\kappa, \kappa_i) = p_n^{L'L'}(\kappa, \kappa_i) \delta_{nn'} + \sum_{n'' (n'' \neq n)} \sum_{L_1 L_2} t_n^{L'L_1}(\kappa, K(E_i)) G_{nn''}^{L_1 L_2}(K(E_i)) \times \mathcal{O}_{nn''}^{L_1 L_2}(K(E_i), \kappa_i) \quad (2.35)$$

As in the LEED problem, only scattering events on the complex energy shell are considered, i.e., $\kappa_i - K(E_i)$, $\kappa - K(E_i)$, and

$$t_n^{L'L}(\kappa(E_i), K(E_i)) = \frac{4\pi i \hbar^2}{mK(E_i)} [\exp(2i\delta_f^n) - 1], \quad (2.36)$$

where the δ_f^n are energy-dependent scattering phase shifts. This turns Eq. (2.35) into a legitimate matrix equation. For a given model of the lattice geometry, the sums over the lattice sites

can be carried out to evaluate the structural propagators.

It is possible to recast the problem as was done in LEED to take advantage of the lattice symmetries, but in the strictest sense, the presence of the excited atom breaks the lattice symmetry and results in a defect problem. Hence, for the model calculations of Sec. III, I will adopt a cluster approach where $\mathcal{O}_{nn'}^{L'L'}$ is determined for a given subset of atoms which surround the excited atom. Because of the inelastic collision damping, only a modest number of atoms will be needed for convergence.

III. MODEL CALCULATIONS

In this section, the importance of multiple-scattering effects is investigated in the context of the isotropic scatterer, inelastic-collision model used in early LEED work.¹⁹ This is a non-trivial question since, although it is clear that multiple-scattering effects are important in interpreting LEED spectra and photoemission from localized adsorbate levels,⁴ it is currently thought that many features of EXAFS spectra can be analyzed via a single-scattering mode.⁵⁻¹⁰ This later feature enables local atomic geometrics to be obtained via simple Fourier transforms of the experimental data without having to resort to complex multiple-scattering calculations. To investigate this aspect of the calculation, I will ignore any energy dependence of the bare excitation matrix elements and take only the S-wave component to be nonzero, i.e.,

$$W_{\uparrow\uparrow(\uparrow\uparrow)}^c = W_{\uparrow\uparrow,00(\uparrow\uparrow)}^{c0} (4\pi)^{-3/2} = \text{const.} \quad (3.1)$$

The electron-single-atom elastic-scattering amplitude is given by

$$t_n^{00}(K(E_i), K(E_i)) = \frac{4\pi i \hbar^2}{mK(E_i)} [\exp(2i\delta_0^n) - 1], \quad (3.2)$$

where the δ_0^n are arbitrarily specified. Assuming a spherically symmetric density of states, the transition rate is

$$\langle \mathcal{O}_I \rangle_s \propto \int_{\mu}^{\infty} dE_f E_f^{1/2} (E_i - \Delta - E_f)^{1/2} \Theta(E_i - \Delta - E_f - \mu) \times \left| 1 + (4\pi)^{1/2} \sum_{n_1} \psi_{n_1}^0(K(E_i)) + \dots + 4\pi \sum_{n_1 n_2} \psi_{n_1}^0(K(E_i)) \psi_{n_2}^{*0}(K(E_f)) + \dots \right. \\ \left. + (4\pi)^{3/2} \sum_{n_1 n_2 n_3} \psi_{n_1}^0(K(E_i)) \psi_{n_2}^{*0}(K(E_f)) \psi_{n_3}^0(K(E_f)) \right|_{E_f = E_i - \Delta - E_f}^2 \quad (3.3)$$

In Eq. (3.3) all energies are referenced with respect to the muffin-tin zero which is V_0 below the vacuum level. This means

$$\hbar^2 K^2(E_i)/2m = E_i - \Sigma(E_i) \quad (3.4)$$

while for the final-state electrons

$$\hbar^2 K^2(E_f)/2m = E_f - \Sigma(E_f) - V_0 \quad (3.5a)$$

$$\hbar^2 K^2(E_{f'})/2m = E_{f'} - \Sigma(E_{f'}) - V_0. \quad (3.5b)$$

The difference between Eqs. (3.4) and (3.5) is because E_i is the incident-beam energy which is specified relative to the vacuum while E_f and $E_{f'}$ are for electrons within the solid and hence do not require the inner potential correction. In Eq. (3.3), μ is the Fermi energy and Θ is the usual step function. Removing the contribution to Eq. (3.3) which would occur for an isolated atom, the geometrical enhancement factor (GEF) due to the surrounding atoms is proportional to

$$\langle \hat{\phi}_I \rangle_s - \int_{\mu}^{\infty} dE_f E_f^{1/2} (E_i - \Delta - E_f)^{1/2} \Theta(E_i - \Delta - E_f - \mu). \quad (3.6)$$

In Fig. 1 I show calculations with parameters corresponding to the excitation of the L_I level in bulk nickel. As an estimate of the core-level binding energy, I use the ESCA value given by Siegbalm *et al.*³⁴ of $E_c = 1008$ eV and correcting this relation to the muffin-tin zero gives $\Delta = 994$ eV. (I take $V_0 = 14$ eV and assume $\mu = 9$ eV after previous LEED work on nickel³¹). In view of the many simplifying assumptions made in Eq. (3.3) any reasonably consistent set of parameters would suffice for the model calculations. This set of calculations neglects multiple-scattering effects and considers only single-scattering events from the atoms in the cluster, i.e.,

$$\phi_{mn}^{L'L'}(K(E_i), K(E_f)) - p_n^{L'L'}(K(E_i), K(E_f)) \delta_{mn}. \quad (3.7)$$

and phase shifts of $\delta = \frac{1}{2}\pi$ are assumed for both the initial and final states. The excited atom is taken to lie at the center of the cluster. The solid line shows the calculated GEF for a cluster consisting of the excited atom and its nearest neighbors. Note that there is only a minimal amount of structure present in this function indicating that the effects of the lattice scattering are largely hidden by the background induced by the final-state summation. However, differentiating with respect to the incident-beam energy, as is done experimentally, yields the lower dashed curve which shows considerable structure. This structure is due primarily to the final-state electrons rather than to the incident electron because of the factor κ^2 which occurs in the denominator of the

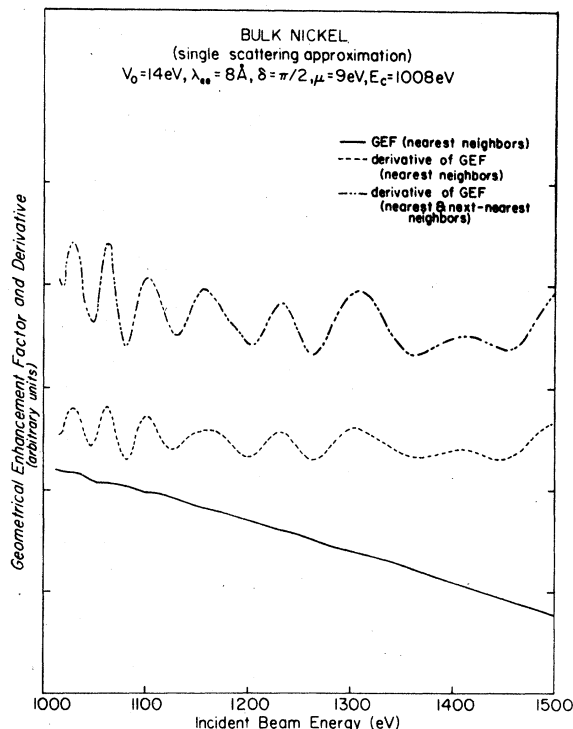


FIG. 1. Calculation of the geometrical enhancement factor (GEF) and its derivative for various clusters of nickel atoms. The calculation is performed in the single-scattering approximation and utilizes the parameters shown in the figure. The solid line shows the GEF for a cluster containing only nearest-neighbor atoms and the lower dashed line shows its derivative with respect to the incident beam energy. The upper dashed line shows the derivative of the GEF when both nearest- and next-nearest-neighbor atoms are included in the cluster.

$\psi^0(\kappa)$. The upper dashed line shows the derivatives of the GEF for a cluster consisting of both nearest and next-nearest neighbors. This curve shows only enhancement of the structure already present for the nearest-neighbor-only case. Hence, in the context of this model calculation it appears that only very short-ranged geometrical information is present in the SXAPS and AEAPS spectra. A more realistic calculation with stronger electron-atom scattering (i.e., more phase shifts) could possibly extend the distance over which geometrical information could be obtained.

To display the effects of multiple-scattering processes, I consider the excitation of any oxygen atom adsorbed on the Ni (001) surface. The cluster of atoms utilized in this series of calculations is shown in Fig. 2. The oxygen atom is assumed to lie in the fourfold symmetric position at a distance d above the outermost plane of nickel atoms.

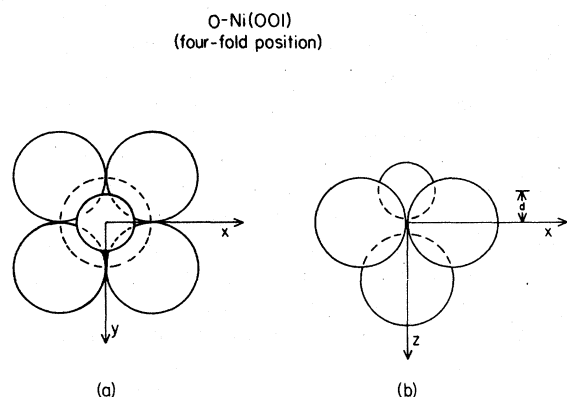


FIG. 2. Atomic cluster used for the O-Ni(001) calculations. The cluster consists of the oxygen atom, the four underlying nickel surface atoms, and the next-nearest-neighbor nickel atom which lies in the second atomic plane. The oxygen atom lies in the four fold symmetric position at a distance d above the nickel surface. (a) shows the projection of the cluster in the x - y plane and (b) shows the projection of the cluster in the x - z plane.

The cluster consists of the oxygen atom, the four underlying nickel atoms, and the next-nearest-neighbor nickel atom which lies in the second plane. This cluster was chosen to minimize the required computation time and more atoms would likely be required to analyze experimental data using a more realistic potential. The Ni-Ni distances are appropriate for an undisturbed surface, i.e., Ni-Ni nearest-neighbor distance equal to 1.76 Å. The binding energy of the oxygen K level from ESCA³⁴ is 532 eV corresponding to a value of $\Delta=518$ eV relative to the muffin-tin zero.

Figure 3 shows the derivatives of the GEF in both the single-scattering approximation and with all multiple-scattering processes included. The lower panel shows curves for the oxygen atom 0.9 Å above the Ni(001) surface and the upper panel shows curves for the oxygen atom 1.2 Å above the Ni(001) surface. Constant scattering phase shifts of $\delta = \frac{1}{2}\pi$ are used for both the oxygen and the nickel atoms in both the initial and final states. Comparing the single-scattering curves, going from $d=1.2$ Å to $d=0.9$ Å shifts the structure in the curves to higher energies consistent with similar shifts observed in LEED calculations when the upper layer spacing is decreased. It is more important, however, to note the changes in the curves on going from the single-scattering approximation to the inclusion of multiple scattering effects. Not only peak shapes but also peak positions are drastically altered. Hence, in the context of this simple model it appears that multiple scattering effects must be included in any analysis of experimental data that requires a di-

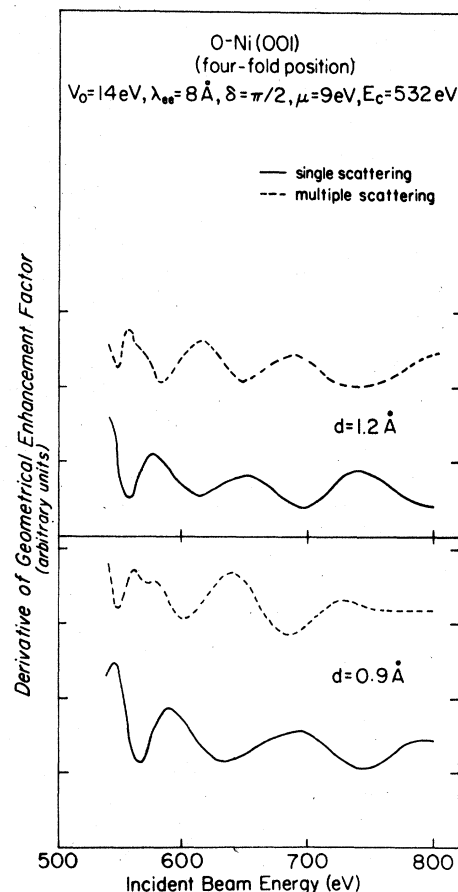


FIG. 3. Derivatives of the GEF for the O-Ni(001) cluster shown in Fig. 2. The solid lines are for the single-scattering approximation while the dashed curves include all multiple-scattering effects. The upper panel is for the oxygen atom 1.2 Å above the Ni(001) surface and the lower panel for the oxygen atom 0.9 Å above the Ni(001) surface. The other parameters used in the calculation are shown in the figure.

rect comparison with theoretical calculations. Presumably, more realistic models for the electron-atom scattering would produce even stronger multiple-scattering corrections. However, Fig. 3 does show the presence of structure which is dependent on the local atomic geometry and so properly analyzed SXAPS and AEAPS data may well yield information about atomic positions in the vicinity of specified atoms.

IV. SUMMARY AND CONCLUSIONS

In summary, I have described a calculation of the structure introduced in SXAPS and AEAPS spectra because of scattering events taking place in the neighborhood of the atom excited by the incident electron beam. This structure depends on the local atomic geometry and its analysis may

provide a way of learning about the local atomic geometry in the region of the excited atom. Unlike the case of LEED, this technique is not restricted to ordered systems. By proper selection of the core levels involved it may be possible to focus on catalytically active sites and not have to determine the entire structure of complex molecular systems. A completely general formalism was described which makes use of the current state of the art of LEED theory for calculating the initial- and final-state electronic wave functions. The problem is more complicated than its counterparts in localized photoemission¹⁻⁴ and EXAFS⁵⁻¹⁰ in that since a high-energy electron is used to excite the atomic core level, there are multiple-scattering events taking place in the initial as well as in the final states and there are no definite selection rules relating the final-state angular momentum to the angular-momentum quantum numbers of the core level. There are also two final-state electrons and so one is left with an explicit sum over final-state energies which tends to smear out the geometrically induced structure. However, differentiating with respect to the incident beam energy brings back this structural information. On the positive side is the fact that SXAPS and AEAPS experiments require only very simple equipment to perform and do not tie the experimentalist to a synchrotron as a continuum source of soft x rays. This advantage may well outweigh the difficulties in analyzing the data. The problem of calculating the bare excitation matrix element was described although no numerical calculations of this quantity were performed. To illustrate the geometrical effects, model calculations were performed in the spirit of the isotropic-scatterer inelastic collision mo-

del used in early LEED work.¹⁹ In the context of those model calculations it appears that the geometrically introduced structure reflects only the positions of the neighboring atoms and that proper inclusion of multiple scattering effects will be important in any direct comparison between theory and experiment. This paper represents only the first step in understanding the phenomenon. Future work will include a more thorough study of the bare excitation matrix element to see how many partial-wave compounds will be necessary to accurately model it and will include a better description of the electron-atom elastic-scattering amplitudes. Work is currently in progress to assess the applicability of Fourier transform techniques to data analysis. It will also be necessary to assess the degree to which uncertainty in specifying the scattering potential of the excited atom will affect extraction of geometrical information and to optimize the cluster size to ensure convergence for a given model potential. However, even in the absence of a complete data analysis, comparison of spectra for both ordered and disordered systems may provide information about changes in adsorbate binding sites. Forthcoming experimental work¹⁸ will provide additional motivation for the theoretical investigations outlined above.

APPENDIX

The "bare" excitation matrix elements are simple generalizations of the atomic physics expressions for the ionization of a hydrogen atom by an incident electron beam.^{27,28} Letting $\phi_c(\vec{r})$ be the wave function of the core electron, the bare matrix element for the two excited-final-state electrons emerging in a triplet state is

$$\begin{aligned}
 W_{\uparrow\uparrow}^c(\vec{k}; \vec{k}_1, \vec{k}_2) &= \frac{(2\pi)^{-9/2}}{2} \int d^3r_1 d^3r_2 \{ \exp[-i(\vec{k}_1 \cdot \vec{r}_1 + \vec{k}_2 \cdot \vec{r}_2)] - \exp[-i(\vec{k}_1 \cdot \vec{r}_2 + \vec{k}_2 \cdot \vec{r}_1)] \} \\
 &\quad \times \frac{e^2}{|\vec{r}_1 - \vec{r}_2|} [\exp(i\vec{k} \cdot \vec{r}_1) \phi_c(\vec{r}_2) - \exp(i\vec{k} \cdot \vec{r}_2) \phi_c(\vec{r}_1)] \\
 &= -W_{\uparrow\uparrow}^c(\vec{k}; \vec{k}_2, \vec{k}_1).
 \end{aligned} \tag{A1}$$

Although I have used a plane-wave basis in order to simplify the coupling to LEED-like wave functions, in actually carrying out a calculation of the bare matrix elements it would be necessary to orthogonalize the plane waves to the core-electron wave function.³⁵ The symmetry properties illustrated in this Appendix are not affected by this orthogonalization procedure. In carrying out the multiple-scattering portion of the calculation it was necessary to utilize a partial-wave expansion of the

excitation matrix element. In performing this expansion I make use of the following partial-wave expansion³²:

$$\begin{aligned}
 \frac{1}{|\vec{r}_1 - \vec{r}_2|} &= \sum_{l=0}^{\infty} \frac{r_{<}^l}{r_{>}^{l+1}} \phi_l(\cos\theta_{12}) \\
 &= 4\pi \sum_L \frac{r_{<}^l}{r_{>}^{l+1}} \frac{1}{2l+1} Y_L^*(\Omega_2) Y_L(\Omega_1).
 \end{aligned} \tag{A2}$$

In Eq. (A2), $r_{<}$ ($r_{>}$) is the lesser (greater) of the

r_1 and r_2 , $\mathcal{P}_l(\cos\theta_{12})$ is the l th Legendre polynomial and θ_{12} is the polar angle between \vec{r}_1 and \vec{r}_2 . I also assume that the atomic core-level wave function can be written as the produce of a radial function and a spherical-harmonic function, i.e.,

$$\phi_c(\vec{r}) = R_{n_c l_c}(r) Y_{L_c}(\Omega), \quad (\text{A3})$$

where n_c is the principal quantum number of the

core-level wave function.

Using Eqs. (A2) and (A3)

$$W_{\uparrow\uparrow}^{c, L}(\vec{k}; \vec{k}_1, \vec{k}_2) = \sum_{L_1 L_2} W_{\uparrow\uparrow, L_1 L_2}^{c, L}(\kappa; \kappa_1, \kappa_2) Y_L(\Omega) \times Y_{L_1}^*(\Omega_1) Y_{L_2}^*(\Omega_2), \quad (\text{A4})$$

where

$$W_{\uparrow\uparrow, L_1 L_2}^{c, L}(\kappa; \kappa_1, \kappa_2) = \frac{16e^2}{\sqrt{2\pi}} \sum_{\bar{L}} \int_0^\infty \int_0^\infty dr_1 dr_2 \frac{r_1^2 r_2^2}{2\bar{L}+1} \frac{r_1^{\bar{L}}}{r_1^{\bar{L}+1}} (i)^{l_1+l_2} \times j_{l_1}(\kappa r_1) R_{n_c l_c}(r_2) [I^*(L; \bar{L}, L_1) I^*(\bar{L}; L_2, L_c) j_{l_1}(\kappa_1 r_1) j_{l_2}(\kappa_2 r_2) - I^*(L; \bar{L}, L_2) I^*(\bar{L}; L_1, L_c) j_{l_1}(\kappa_1 r_2) j_{l_2}(\kappa_2 r_1)]. \quad (\text{A5})$$

The important things to notice about Eq. (A5) are the following symmetry properties:

$$W_{\uparrow\uparrow, L_1 L_2}^{c, L}(-\kappa; \kappa_1, \kappa_2) = (-1)^l W_{\uparrow\uparrow, L_1 L_2}^{c, L}(\kappa; \kappa_1, \kappa_2), \quad (\text{A6})$$

$$W_{\uparrow\uparrow, L_1 L_2}^{c, L}(\kappa; -\kappa_1, \kappa_2) = (-1)^{l_1} W_{\uparrow\uparrow, L_1 L_2}^{c, L}(\kappa; \kappa_1, \kappa_2), \quad (\text{A7})$$

$$W_{\uparrow\uparrow, L_1 L_2}^{c, L}(\kappa; \kappa_1, -\kappa_2) = (-1)^{l_2} W_{\uparrow\uparrow, L_1 L_2}^{c, L}(\kappa; \kappa_1, \kappa_2). \quad (\text{A8})$$

Similarly, the "bare" excitation matrix element for the two excited-final-state electrons emerging in a singlet state is given by

$$W_{\uparrow\uparrow}^c(\vec{k}; \vec{k}_1, \vec{k}_2) = \frac{(2\pi)^{-9/2}}{2} \int d^3 r_1 d^3 r_2 \{ \exp[-i(\vec{k}_1 \cdot \vec{r}_1 + \vec{k}_2 \cdot \vec{r}_2)] + \exp[-i(\vec{k}_1 \cdot \vec{r}_2 + \vec{k}_2 \cdot \vec{r}_1)] \} \times \frac{e^2}{|\vec{r}_1 - \vec{r}_2|} [\exp(i\vec{k} \cdot \vec{r}_1) \phi_c(\vec{r}_2) + \exp(i\vec{k} \cdot \vec{r}_2) \phi_c(\vec{r}_1)] = W_{\uparrow\uparrow}^c(\vec{k}; \vec{k}_2, \vec{k}_1). \quad (\text{A9})$$

As in the case of antiparallel spins, a partial-wave expansion of Eq. (A9) yields

$$W_{\uparrow\uparrow}^c(\kappa; \kappa_1, \kappa_2) = \sum_{L_1 L_2} W_{\uparrow\uparrow, L_1 L_2}^{c, L}(\kappa; \kappa_1, \kappa_2) Y_L(\Omega) Y_{L_1}^*(\Omega_1) Y_{L_2}^*(\Omega_2), \quad (\text{A10})$$

where

$$W_{\uparrow\uparrow, L_1 L_2}^{c, L}(\kappa; \kappa_1, \kappa_2) = \frac{16e^2}{\sqrt{2\pi}} \sum_{\bar{L}} \int_0^\infty \int_0^\infty dr_1 dr_2 \frac{r_1^2 r_2^2}{2\bar{L}+1} \frac{r_1^{\bar{L}}}{r_1^{\bar{L}+1}} (i)^{l_1+l_2} \times j_{l_1}(\kappa r_1) R_{n_c l_c}(r_2) [I^*(L; \bar{L}, L_1) I^*(\bar{L}; L_2, L_c) j_{l_1}(\kappa_1 r_1) j_{l_2}(\kappa_2 r_2) + I^*(L; \bar{L}, L_2) I^*(\bar{L}; L_1, L_c) j_{l_1}(\kappa_1 r_2) j_{l_2}(\kappa_2 r_1)]. \quad (\text{A11})$$

As is the case of parallel spins, the partial-wave components have the following symmetry properties:

$$W_{\uparrow\uparrow, L_1 L_2}^{c, L}(-\kappa; \kappa_1, \kappa_2) = (-1)^l W_{\uparrow\uparrow, L_1 L_2}^{c, L}(\kappa; \kappa_1, \kappa_2); \quad (\text{A12})$$

$$W_{\uparrow\uparrow, L_1 L_2}^{c, L}(\kappa; -\kappa_1, \kappa_2) = (-1)^{l_1} W_{\uparrow\uparrow, L_1 L_2}^{c, L}(\kappa; \kappa_1, \kappa_2); \quad (\text{A13})$$

$$W_{\uparrow\uparrow, L_1 L_2}^{c, L}(\kappa; \kappa_1, -\kappa_2) = (-1)^{l_2} W_{\uparrow\uparrow, L_1 L_2}^{c, L}(\kappa; \kappa_1, \kappa_2) \quad (\text{A14})$$

Note added in proof: Additional work indicates that in the context of the S-wave scattering model the main effect of multiple-scattering processes is to introduce an overall "phase shift" with respect to curves for the GEF calculated in the

single-scattering limit. This shift makes curves calculated in the two limits look quite different but does not affect a Fourier transform process. Hence, just as in EXAFS, Fourier transform techniques may be useful in data analysis.³⁶

- ¹B. J. Wacławski, T. V. Vorburger, and R. J. Stein, *J. Vac. Sci. Technol.* **12**, 301 (1975).
- ²W. F. Egelhoff and D. L. Perry, *Phys. Rev. Lett.* **34**, 93 (1975).
- ³J. W. Gadzuk, *Solid State Commun.* **15**, 1011 (1974); *Phys. Rev. B* **10**, 5030 (1974).
- ⁴A. Liebsch, *Phys. Rev. B* **13**, 544 (1976); *Phys. Rev. Lett.* **38**, 248 (1977).
- ⁵L. V. Azaroff, *Rev. Mod. Phys.* **35**, 1012 (1963).
- ⁶D. E. Sayers, E. A. Stern, and F. W. Lytle, *Phys. Rev. Lett.* **27**, 1204 (1971).
- ⁷D. E. Sayers, F. W. Lytle, and E. A. Stern, in *Advances in X-ray Analysis*, edited by B. L. Henke, J. B. Newkirk, and G. R. Mallett (Plenum, New York, 1970).
- ⁸W. L. Schaich, *Phys. Rev. B* **8**, 4028 (1973); **14**, 4420 (1976).
- ⁹P. A. Lee and J. B. Pendry, *Phys. Rev. B* **11**, 2795 (1975).
- ¹⁰J. J. Rehr and E. A. Stern, *Phys. Rev. B* **14**, 4413 (1976).
- ¹¹C. B. Duke, in *Dynamic Aspects of Surface Physics*, edited by F. O. Goodman (Editrice Compositori, Bologna, 1974).
- ¹²J. B. Pendry, *Low Energy Electron Diffraction* (Academic, New York, 1974).
- ¹³R. L. Park, J. E. Houston, and D. G. Schreiner, *Rev. Sci. Instrum.* **41**, 1810 (1970).
- ¹⁴J. E. Houston and R. L. Park, *J. Vac. Sci. Technol.* **8**, 91 (1971).
- ¹⁵R. L. Park and J. E. Houston, *J. Vac. Sci. Technol.* **11**, 1 (1974).
- ¹⁶R. L. Park and M. den Boer, *CRC Crit. Rev. Solid State Sci.* **6**, 275 (1976), and the references therein.
- ¹⁷J. E. Houston and R. L. Park, *Phys. Rev. B* **5**, 3808 (1972).
- ¹⁸The question obviously arises as to whether these effects have been previously noted in existing experimental data. In general, the predicted structure occurs over a fairly wide energy range and the published experimental data on clean systems is only over a fairly narrow energy range in order to show the details of density of states effects. Data over a large energy range is generally on fairly contaminated systems where it is difficult to separate the structure due to the impurities from that due to geometrical phenomenon. However, J. E. Houston and R. L. Park, *J. Chem. Phys.* **55**, 4601 (1971), Fig. 8, show structure which may be due to geometrical phenomena.

Also, R. L. Park, in 24th National Symposium of the American Vacuum Society and private communication, reports structure on clean, well-characterized systems which illustrates the effects described in this paper.

- ¹⁹C. B. Duke and C. W. Tucker, Jr., *Phys. Rev. Lett.* **23**, 1163 (1969); *Surf. Sci.* **15**, 231 (1969).
- ²⁰C. B. Duke and G. E. Laramore, *Phys. Rev. B* **2**, 4765 (1970).
- ²¹G. E. Laramore and C. B. Duke, *Phys. Rev. B* **2**, 4783 (1970).
- ²²G. E. Laramore, *Phys. Rev. Lett.* **27**, 1050 (1971).
- ²³D. C. Langreth, *Phys. Rev. Lett.* **26**, 1229 (1971).
- ²⁴G. E. Laramore, *Solid State Commun.* **10**, 85 (1972).
- ²⁵F. Herman and S. Skillman, *Atomic Structure Calculations* (Prentice-Hall, Englewood Cliffs, N.J., 1963).
- ²⁶D. Liberman, J. T. Waber, and D. T. Cromer, *Phys. Rev.* **137**, A27 (1965).
- ²⁷M. R. H. Rudge, *Rev. Mod. Phys.* **40**, 564 (1968).
- ²⁸F. W. Byron, Jr. and C. J. Joachain, *Phys. Rev. A* **8**, 1267 (1973).
- ²⁹G. E. Laramore and C. B. Duke, *Phys. Rev. B* **5**, 267 (1972).
- ³⁰M. E. Rose, *Elementary Theory of Angular Momentum* (Wiley, New York, 1967), p. 62. An explicit expression for $I(L_j, L_1, L_2)$ is also given in Ref. 21.
- ³¹G. E. Laramore, *Phys. Rev. B* **8**, 515 (1973).
- ³²See, for example, J. D. Jackson, *Classical Electrodynamics* (Wiley, New York, 1963), Chap. 3.
- ³³This follows from the symmetry properties of $W_{\uparrow\uparrow}^{L_1 L_2}(\kappa; \vec{\kappa}_f, \vec{\kappa}_{f'})$ as defined in Eq. (A5), the symmetry properties of the $j_i(\kappa R_n)$, and the symmetry properties of the electron-single-atom scattering amplitudes as illustrated in Ref. 21. That is
- $$W_{\uparrow\uparrow}^{L_1 L_2}(-\kappa; \vec{\kappa}_f, \vec{\kappa}_{f'}) j_{i_1}(-\kappa R_n) \mathcal{P}_{m_i}^{L_2 L_3}(-\kappa, \kappa_i) \\ = (-1)^{l_1 + l_2} W_{\uparrow\uparrow}^{L_1 L_2}(\kappa; \vec{\kappa}_f, \vec{\kappa}_{f'}) \\ \times j_{i_1}(\kappa R_n) \mathcal{P}_{m_i}^{L_2 L_3}(\kappa, \kappa_i).$$
- ³⁴K. Siegbahn, C. Nordling, A. Fahlman, R. Nordbeny, K. Hamrin, J. Hedman, G. Johansson, T. Boegnark, S. Karlsson, I. Lindgren, and B. Lindberg, *ESCA: Atomic Molecular and Solid State Structure Studied by Means of Electron Spectroscopy* (Almqvist and Wiksells, Uppsala, 1967), Appendix I.
- ³⁵T. L. Einstein (private communication).
- ³⁶G. E. Laramore, *Surface Sci.* (to be published).